Rate-Determining Factors in the Chain Polymerization of Molecules Initiated by Local Single-Molecule Excitation

Swapan K. Mandal,* Yuji Okawa, Tsuyoshi Hasegawa, and Masakazu Aono

International Center for Materials Nanoarchitectonics (MANA), National Institute for Materials Science (NIMS), 1-1 Namiki, Tsukuba, Ibaraki 305-0044, Japan

ABSTRACT Spontaneous chain polymerization of molecules initiated by a scanning tunneling microscope tip is studied with a focus on its rate-determining factors. Such chain polymerization that happens in self-assembled monolayers (SAM) of diacetylene compound molecules, which results in a π-conjugated linear polydiacetylene nanowire, varies in its rate *P* depending on domains in the SAM and substrate materials. While the arrangement of diacetylene molecules is identical in every domain on a graphite substrate, it varies in different domains on a MoS_2 substrate. This structural variation enables us to investigate how *P* is affected by molecular geometry. An important determining factor of *P* is the distance between two carbon atoms which are to be bound by polymerization reaction, *R*; as *R* decreases by 0.1 nm, *P* increases ~2 times. *P* for a MoS_2 substrate is ~4 times higher (with the same value of *R*) than that for a graphite substrate because of higher mobility of molecules. The exciting correlation of the chain polymerization rate to the geometrical structure of the diacetylene molecules brings a deeper understanding of the mechanism of chain polymerization kinetics. In addition, the fabrication of one-dimensional conjugated polymer nanowires on a semiconducting MoS_2 substrate as demonstrated here may be of immense importance in the realization of future molecular devices.

KEYWORDS: chain polymerization rate · polymer nanowire · scanning tunneling microscopy · polydiacetylene · molybdenum disulfide

Scanning tunneling microscope (STM) probe tip-induced chain polymerization[1−4] is an elegant and versatile technique to obtain one-dimensional (1-D) conjugated polymer nanowires. The chain polymerization can be initiated at designated positions with easy processability and functionality, removing many constraints for fabrication and integration of molecular devices. This spontaneous chain polymerization is instigated by a local single-molecule excitation using the STM probe tip upon application of a certain voltage pulse to a self-assembled monolayer (SAM) of a diacetylene compound (DA; general formula $R_1-C\equiv C-C\equiv C-R_2$, where $C\equiv C-C\equiv C$ is the diacetylene moiety, R_1 and R_2 are substituent groups) and has been successfully demonstrated for fabricating polydiacetylene (PDA; $(=R_1C-C\equiv C-CR_2=)_n$) nanowires on a highly oriented pyrolytic graphite (HOPG) substrate.[1−4] The PDA nanowire thus obtained is a conjugated linear polymer of submicrometer length. Following charge carrier injection by chemical doping[5] or by applied electric field,[6,7] the PDA nanowire functions as an electrically conductive nanowire. Individual PDA nanowires serve as exciting templates for interesting fundamental studies,[5,6,8,9] and PDA also has many potential applications such as in switching devices, transistors, and photovoltaics.[7,10] Fabrication and manipulation of polymer nanowires on suitable substrates may find wide applications in the rapidly developing field of single-molecule electronic elements and devices.[11−21] Although the technique of chain polymerization by STM tip-induced voltage pulse is well-established, the very intriguing question on the rate of chain polymerization still remains unanswered. The polymerization rate we define here is the probability of initiating the chain polymerization process upon application of pulsed bias voltage by the STM tip. Quite reasonably, the intriguing question remains "what are the rate-determining factors in the chain polymerization process"? Relation between the polymerization reactivity and the packing parameters has been reported for solid-state crystals of many diacetylene compounds having various substituent groups.[22] However, it was difficult to distinguish the effect of different packing parameters and the effect of different substituent groups. It was also difficult to discuss the individual processes of chain polymerization because the reaction was monitored as the averaged value for whole crystals. Here, we investigate the polymerization rate of a single event of chain polymerization using local single-molecule excitation on SAMs of DA which have the same substituent group but have different molecular arrangement. From this investigation, we establish the key factors which determine the polymerization rate. This establishment further brings a deeper understanding of the whole process of polymerization kinetics which is very much necessary to fully exploit

* Address correspondence
sk_mandal@hotmail.com.

Received for review November 28, 2010 and accepted March 14, 2011.

Published online March 14, 2011
10.1021/nn103231j

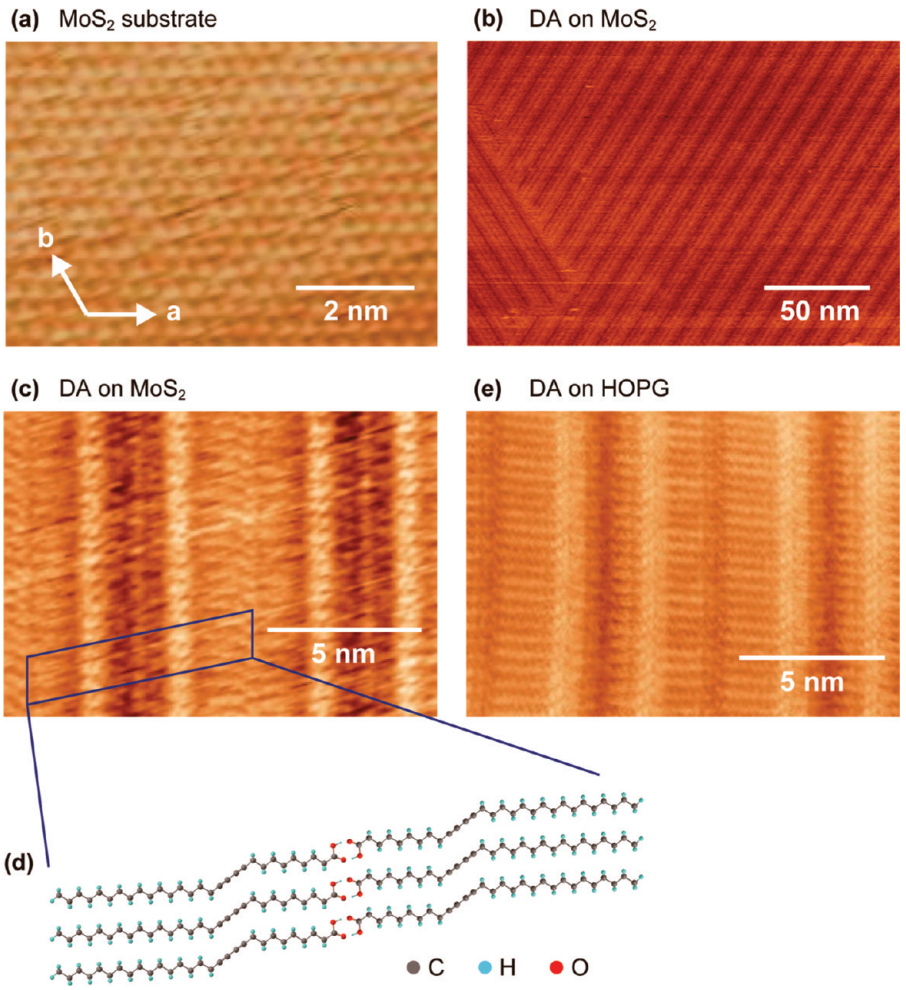

Figure 1. STM images of (a) atomically resolved bare MoS_2 substrate [(a,b) gives the direction of the lattice vectors], (b,c) SAM of DA on MoS_2 substrate. (d) Schematic view of the molecular arrangement of DA and (e) STM image of SAM of DA on graphite substrate.

the versatility of the technique in molecular device fabrication.

On the other hand, despite its simplicity and versatility, STM tip-induced polymerization has thus far only been demonstrated on a conducting HOPG substrate. The process still needs to be demonstrated and investigated on other semi-insulating or insulating substrates. Fabrication of 1-D conjugated polymer nanowires on semiconducting or insulating substrates[23] rather than (semi-) metallic substrates will enable further elucidation of electrical properties of nanowires and physics of 1-D systems. The choice of a suitable substrate is crucial for fabricating molecular nanodevices. We therefore describe here the crucial role of the substrate in determining the molecular arrangements of DA and in turn the polymerization rate by comparing the results obtained on both HOPG and MoS_2 substrates. Although both MoS_2 and HOPG can be cleaved easily to give atomically flat and inert surfaces, MoS_2 being a moderate band gap semiconductor ($\sim$1.2 eV)[24] seems to be a better substrate on which to study various physical properties of PDA than metallic HOPG. Apart from being a semiconductor, MoS_2 also has a larger lattice constant (0.316 nm) and greater work function (4.6 to 4.9 eV) compared with (semi-) metallic HOPG (lattice constant 0.246 nm and work function 4.48−4.6 eV).[9,24] Also, different surface atoms (S on MoS_2 and C on HOPG) may give different chemical interactions with the adsorbed molecules. Photopolymerization of DA on a MoS_2 substrate has been reported,[9] but STM tip-induced polymerization has yet to be demonstrated. In this paper, we successfully fabricate conjugated polymer nanowires on MoS_2 substrate by STM tip-induced polymerization of DA and also find that the rate of polymerization is significantly enhanced on MoS_2 substrate in comparison to HOPG.

RESULTS AND DISCUSSION

Understanding of the whole process of polymerization kinetics of DA is necessary to fully exploit the versatility of the STM tip-induced polymerization technique. Moreover, fabrication of conjugated polymer nanowires on insulating or semiconducting substrates is very important for further elucidation of electrical properties of polymer nanowires as well as for realization of molecular electronics. Such a possibility is being demonstrated here using a SAM of DA on a MoS_2 substrate. Besides fabrication of conjugated polymer nanowires on a MoS_2 substrate, the

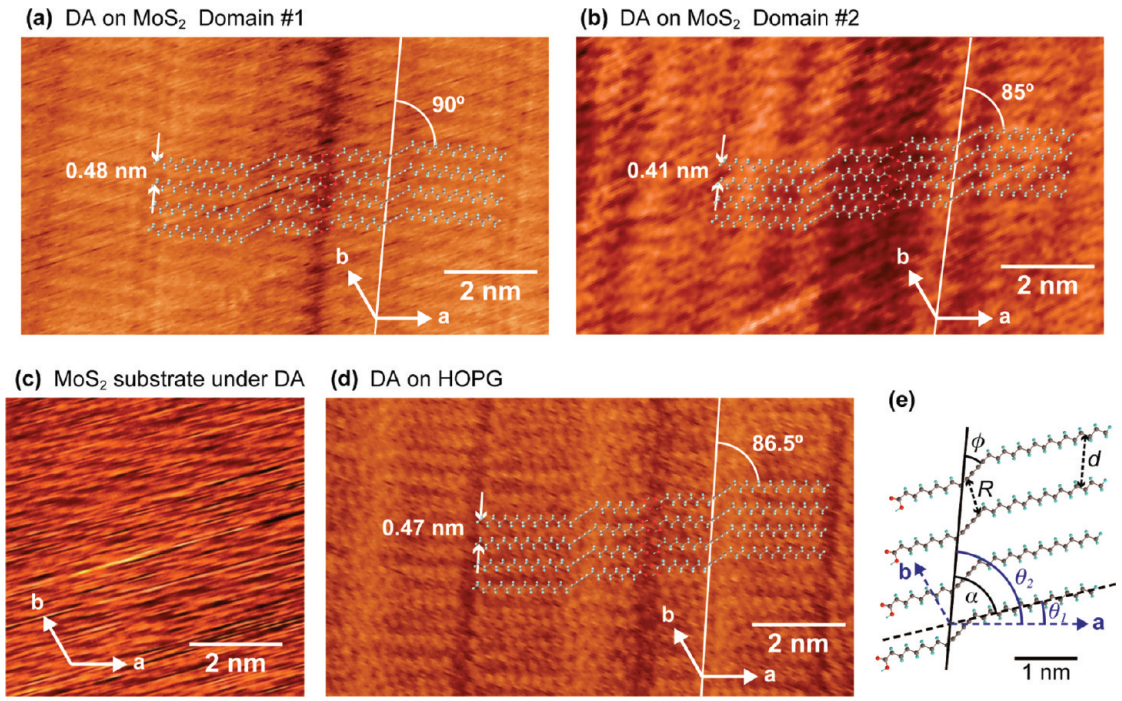

Figure 2. High-resolution STM images of (a,b) DA layer of two different domains on MoS_2 substrate, (c) MoS_2 substrate lattice under DA layer (sample bias −0.35 V, tunneling current 1 nA), (d) DA layer on HOPG substrate (sample bias −0.6 V, tunneling current 25 pA). Superimposed molecular models indicating the molecular geometry on the DA layer are also given within (a,b) and (d). (e) Schematic sketch of the molecular arrangement of DA indicating the structural parameters *d*, *R*, α, θ_1, θ_2, and ϕ (as defined in the text); α and *d* are also specified within superimposed molecular models in panels (a,b) and (d). The directions of the underlying substrate lattice vectors (a,b) are also presented in the inset of (a−e). The solid white lines in (a,b) and (d) indicate the directions of molecular rows.

effect of substrate-specific molecular mobility and geometry on the polymerization kinetics and polymerization rate is discussed, as it has not been reported before. We believe that the results presented here seem to be quite interesting and have far reaching impetus in the field of molecular electronics as well as exploration of material physics in one dimension and macromolecular sciences.

We use 10,12-nonacosadiynoic acid ($CH_3(CH_2)_{15}$−C≡C−C≡C−$(CH_2)_8$COOH) as the DA. Figure 1a shows an atomically resolved STM image of a freshly cleaved MoS_2 substrate surface. The DA molecular layer deposited on the substrate is, in general, self-assembled into several domains with typical domain sizes of 100−300 nm. In Figure 1b, we present the typical STM topographical image of a DA layer containing two different domains, which clearly shows the growth of 1-D molecular chains of DA on the MoS_2 substrate. We also present a high-resolution STM image of the SAM on MoS_2 in Figure 1c, where the vertical bright lines correspond to the aligned diacetylene moieties (see Figure 1d). The molecular arrangement of Figure 1c appears similar to that obtained on HOPG substrate, as shown in Figure 1e.[2] The molecules lie flat on both substrates, aligned to form straight chains, and the chains are arranged in a manner such that −COOH end groups of a chain are opposite those of a neighboring chain (Figure 1d). However, we find two striking differences between the molecular layers on these two substrates.

First, the resolution of the STM images of DA is usually higher on HOPG than on MoS_2, as observed in the typical images shown in Figure 1c,e. While atomic resolution is frequently attained for DA on HOPG, only molecular or submolecular resolution is usually obtained on MoS_2. Since we have examined more than 100 images of DA on MoS_2 and HOPG, this effect is unlikely to be because of differences in STM tip condition. Rather, it is an indication of the weaker interaction of alkyl side chains with MoS_2 than with HOPG, giving rise to a greater mobility of the molecular layer in the former case. A similar tendency is also reported for many other alkyl derivative molecules on MoS_2 and HOPG.[25] This observation is consistent with a previous report that the heat of adsorption of *n*-dotriacontane on MoS_2 is approximately one-third of the value obtained on graphite.[26]

Second, we find that the arrangement of DA (intermolecular spacing and angles) varies in different domains on MoS_2 but remains constant on HOPG. To investigate this, we have first obtained high-resolution STM images of the DA layer within various domains of the same sample (Figure 2a,b), while simultaneously recording an atomic image of the underlying MoS_2 substrate lattice (Figure 2c). This is done by suitably tuning the tunneling current and the sample bias voltages without changing the scanning area and scanning speed.[27] We use the substrate lattice image to accurately calibrate the structural parameters of the arrangement of DA and to find the relationship between the arrangement of DA

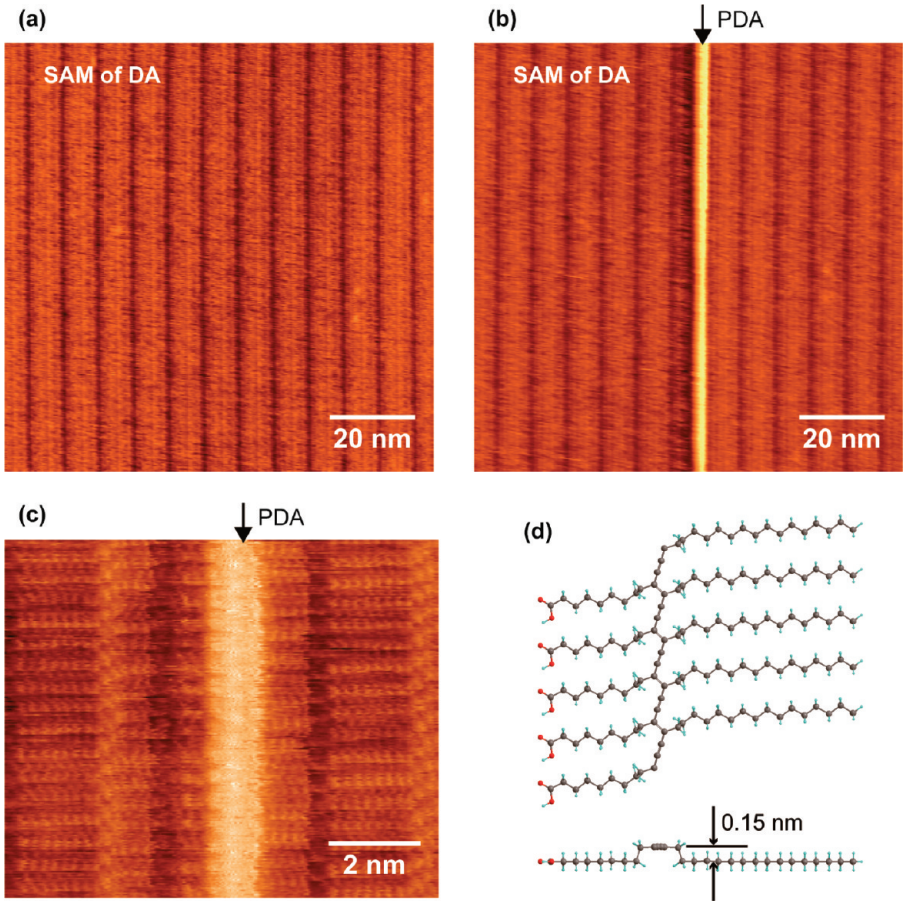

Figure 3. STM images of DA layer on MoS_2 (a) before and (b) after chain polymerization. The polymerization is done by applying pulsed sample bias ($V_s = -3.5$ V, 5 μs width) through the STM tip. The fabricated PDA is seen as a bright line in (b). (c) Section of the high-resolution image of the PDA. A schematic diagram of the lifted-up conformation model of PDA is presented in (d) with top and side view.

and the substrate lattice. Besides two representative images of DA in two different domains on MoS_2 (Figure 2a,b), for comparison, we also provide an image of DA on HOPG in Figure 2d. In the domain shown in Figure 2a, the measured spacing d between neighboring molecules along the direction of the molecular row (see Figure 2e) is 0.48 $\pm$ 0.01 nm. The angle θ_1 between the direction of the alkyl side chains and the direction of a main crystal axis (**a**) of the MoS_2 substrate is $-5 \pm 2°$, and the angle θ_2 between the direction of the molecular row and that of a main crystal axis (**a**) of the MoS_2 substrate is 85 $\pm$ 1°. The angle α between the direction of alkyl side chains and the direction of the molecular row is thus obtained as 90 $\pm$ 2° ($\alpha = \theta_2 - \theta_1$). In another domain shown in Figure 2b, the structural parameters d, θ_1, θ_2, and α are measured to be 0.41 $\pm$ 0.01 nm, $-2 \pm 2°$, 83 $\pm$ 1°, and 85 $\pm$ 2°, respectively, different from those in Figure 2a. In total, we measured 19 domains on MoS_2 and found significant variations: d varied from 0.41 to 0.48 nm, θ_1 from -7 to 7°, θ_2 from 83 to 96°, and α from 85 to 95°. In contrast to the case of MoS_2 described above, the direction of alkyl side chains of DA on HOPG is always parallel to the main crystal axis of graphite ($\theta_1 = 0°$). The other structural parameters of DA on HOPG are also constant, d = 0.474 nm, $\theta_2 = \alpha$ = 86.5°, irrespective of domains (see Figure 2d).[2] It further supports the idea of weaker interaction of alkyl side chains with MoS_2 than with HOPG. Probably this is further related to the lattice mismatch: the length of an alkane's C−C−C zigzag, 0.251 nm, is only 2% longer than the lattice constant of HOPG, 0.246 nm, but different from that of MoS_2, 0.316 nm. Also note that the variations of θ_1 and θ_2 for DA on MoS_2 are not random. This indicates that, although the interaction between the adsorbed DA molecule and the lattice of MoS_2 substrate is very weak, it exists to some extent.

Giridharagopal and Kelly[9] have reported that the angles between the directions of molecular rows in different domains are 5−7° on HOPG and 11−13° on MoS_2, which they called "misfit angles". We must note that these misfit angles do not directly correspond to the variation of θ_2 because we should consider equivalent mirror domains. For instance, in the case of HOPG (θ_2 = 86.5°), the angle between the direction of molecular rows of a domain and an equivalent mirror domain flipped along **a** is 7° (=180° $- 2\theta_2$). Similarly, the angle between the directions of molecular rows in different domains will vary from 0 to 14° on MoS_2, where 14° is the angle between the directions of molecular rows of a domain of θ_2 = 83° and an equivalent mirror domain. These angles may correspond to the reported misfit angles.

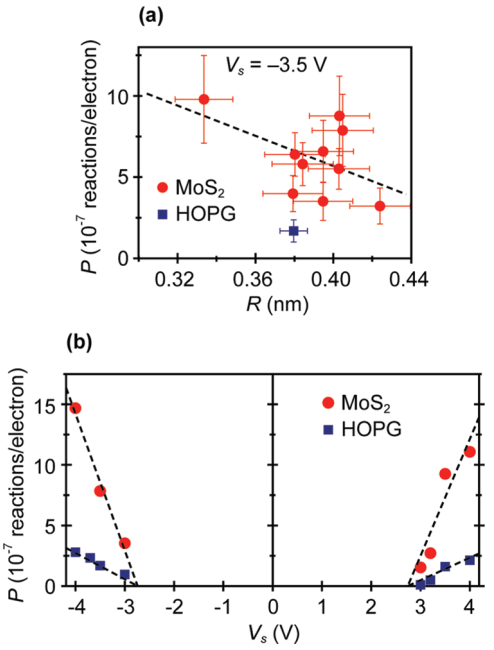

Figure 4. Plots of tip-induced polymerization rate *P* per tunneling electron measured both on MoS_2 and HOPG substrates. (a) Plot of *P* against the reactive carbon−carbon distance *R* (as defined in the text) measured using pulsed sample bias voltage of height $V_s = -3.5$ V and width 5 μs. (b) Plot of *P* against V_s for a constant width of 5 μs. The dashed lines are guides to the eye.

Application of pulsed bias by positioning the STM probe tip into any DA row on the MoS_2 substrate results in the formation of a PDA nanowire through a chain polymerization process, similar to the case of DA on HOPG.[1−4] Figure 3a,b shows the STM images obtained before and after the application of a pulsed sample bias voltage (height $V_s = -3.5$ V, width 5 μs), respectively. The PDA nanowire can be clearly seen as the bright line in Figure 3b. The very high-resolution image of the PDA on MoS_2 in Figure 3c shows no change in orientation of alkyl side chains or rest of the monomer upon application of pulsed bias, as observed also for DA on HOPG. The fact that the alkyl chain orientation is not modulated by the polymerization indicates the lifted-up conformation model (Figure 3d) for PDA on MoS_2, as previously found for PDA on HOPG.[2,28]

Next, we discuss the rate of tip-induced chain polymerization of DA as defined by the reaction probability per tunneling electron, *P*. As mentioned above, different domains of DA on a MoS_2 substrate have different molecular geometries. Hence we have an opportunity to investigate how reaction probability is affected by molecular geometry. First we determine the structural parameters of the DA layer on a selected domain by comparing with the atomic image of the underlying MoS_2 substrate lattice as discussed above. After recording the substrate lattice image, one can revert back to the DA layer by adjusting the tunneling current and sample bias voltage to the original value. Then the polymerization rate measurements are done for that particular domain by applying pulsed bias voltages ($V_s = -3.5$ V, 5 μs width) more than 50 times on the same domain and counting how many chain polymerizations are initiated. The tunneling current is monitored during the application of the pulsed bias voltage, which is typically about 30 nA. The estimation of reaction probability per tunneling electron, *P*, usually requires one to measure, for each event, the time before the reaction occurs.[29,30] Instead, we simply measure the probability of reaction during a given time duration of pulse (5 μs) and then calculate *P* as $P = 1 - (1 - n_c/n_t)^{1/n}$, where n_t is the total number of pulses applied using the STM tip, n_c is the number of pulses that initiate the successful chain polymerization reaction, and *n* is the number of electrons in one pulse which can be estimated from the tunneling current and the time duration of pulse. The details of the calculation of *P* are given in the Supporting Information.

The geometry of diacetylene compounds is conventionally described by parameters *d*, ϕ, and *R*,[22] where ϕ is the angle between the direction of the diacetylene moiety and the direction of the molecular row, and *R* is the distance between two reactive carbon atoms which are to be bound by polymerization reaction process (see Figure 2e). *R* is a crucial parameter for the reaction probability—shorter *R* is expected to lead to higher *P*. From the geometry of DA molecules depicted in Figure 2e, *R* is related to *d* and ϕ by $R^2 = d^2 + l^2 - 2dl\cos\phi$, where *l* is the length of the diacetylene moiety (C≡C−C≡C) estimated to be 0.383 nm using a semiempirical calculation. Assuming that the sp^3 bond angle of carbon is 109.5°, ϕ can be estimated from α: $\phi = \alpha - 90° + 109.5°/2$. Hence, a plot of *P* against *R* can be obtained by measuring *d*, α, and *P* on various domains, as shown in Figure 4a.

This plot shows a distinct increase in *P* with decrease in *R*, in a somewhat linear manner (indicated by the dashed line). Here, the DA molecule may have the cross section for the excitation, namely, the DA molecule may have an excitation probability depending on the stimulating position where electrons are injected. Since we cannot precisely control the position of electron injection at atomic resolution, *P* on a denser molecular layer may be observed to be higher. From the variation of *d* (0.41−0.48 nm), this effect is roughly estimated to be ~15%. Hence, even if we consider this effect of cross section, we can conclude that as *R* decreases by 0.1 nm and *P* increases by a factor of ~2. This correlation between reaction probability *P* and reactive carbon−carbon distances *R* provides deep insight into the mechanism of the STM tip-induced polymerization process as discussed later.

We also measure *P* of DA on a HOPG substrate (average of several measurements is plotted by the blue square point in Figure 4a). As mentioned before, every DA domain on HOPG has the same structural parameters with $R = 0.38$ nm for all domains. This plot shows that the polymerization rate of DA on MoS_2 is remarkably higher (about 4 times) as compared to DA on HOPG with the same value of *R*. Next, we measure *P* as a function of applied pulsed bias V_s on typical domains of DA on both MoS_2 and HOPG. The data are collected at a fixed pulse width of 5 μs while monitoring

the tunneling current during application of the pulsed bias, and the reaction probability per tunneling electron P is plotted in Figure 4b. This plot shows that dependence of P upon V_s is very similar on both MoS_2 and HOPG except that the absolute values of P are different. The P on MoS_2 is much higher (4−6 times) than that on HOPG for all V_s values used here. The plot is nearly symmetric with respect to the polarity of V_s, and the threshold kinetic energy of tunneling electrons to initiate chain polymerization is the same for both substrates, 2.7 ± 0.2 eV. This suggests that the reaction mechanism on both substrates is essentially the same.

It is to be noted that resonant tunneling through occupied and unoccupied orbitals of adsorbed organic molecules, which are extensively observed in inelastic electron tunneling spectra (IETS),[31−34] shows highly biased polarity dependence. Hence, the observed symmetric dependence of P indicates that the resonant tunneling through the orbitals of DA does not directly initiate the chain polymerization. The symmetric dependence of P also suggests that the chain polymerization is not initiated by the charge injection to DA by the electric field. In addition, the reported value of the activation energy is about 1 eV for thermal polymerization of the DA bulk crystal,[35] which does not correspond to the threshold energy of 2.7 eV observed in Figure 4b. Instead, this threshold value essentially corresponds to the reported value of the difference in energy between the $\pi-\pi$ ground state and the lowest excited $\pi-\pi^*$ triplet state of the diacetylene moiety (~3.1 eV).[36] Hence, it is a reasonable assumption that the formation of an electronically excited state of DA is the first stage of chain polymerization: electrons tunneling from the tip to the substrate (for positive V_s) or from the substrate to the tip (for negative V_s) pass inelastically through the DA layer and excite the diacetylene moiety. It is reported by many authors previously that the $\pi-\pi^*$ excited state of DA is the chain initiation species,[35,37] and inelastic excitations from $\pi-\pi$ singlet to $\pi-\pi^*$ triplet state of organic molecules were sometimes observed in IETS.[33,38,39]

The process of chain polymerization is then considered as follows.[2,37] Once the single diacetylene moiety is locally excited, this creates a diradical state with an unpaired electron at either end of the moiety. The excited state either relaxes into the underlying substrate or triggers additional induced reactions. The former does not produce polymerization, while the latter may initiate the chain polymerization reaction. Within the lifetime of the diradical state, an addition reaction takes place, forming a dimer of diacetylene if a neighboring diacetylene moiety approaches one side of the diradical by thermal vibrations. Now, since the created dimer is still in its excited state with an unpaired electron at both ends, similar addition reactions can be induced on either side, repetition of which results in an extended π-conjugated chain-polymerized state of PDA. Since the lifetime of the dimer or oligomer is much longer than the lifetime of the diradical state of the monomer (~10^{-8} s), the probability of chain polymerization is greatly influenced by whether the first addition reaction is able to occur within the lifetime of the diradical state. The addition reaction will be more probable in the case of shorter distances R between the reactive carbon ends (primarily governed by the molecular geometry on the substrate) and is clearly proved in Figure 4a. Apart from these, since the molecules on the MoS_2 surface are more mobile as discussed before, they experience greater thermal vibrations than on HOPG. This increases the frequency of approach of diacetylene moieties favoring dimer formation and hence promotes chain polymerization reaction on MoS_2 substrate compared with HOPG. It is worthwhile to mention that, besides proximity of reactive carbon atoms, the lifetime of the excited state of the molecules may also influence the reaction probability. However, in our case, the lifetime of the excited states is presumably similar on both HOPG and MoS_2 substrates. Since the threshold voltage of the reaction is the same for both the substrates, ~ 2.7 V, it can be concluded that the electronic state of DA is identical on both HOPG and MoS_2. This means that the different interactions between alkyl side chains and the substrates, which is discussed before, do not affect the electronic state of the diacetylene moieties of molecules. This further suggests that the electronic coupling of diacetylene moieties to both the substrate are essentially similar and, therefore, the excited state lifetime, too.

CONCLUSIONS

In conclusion, we find that substrate-specific molecular mobility and geometry are the important factors to determine tip-induced chain polymerization rate of DA. A direct correlation of the polymerization rate with the molecular mobility and geometry brings a clearer understanding of the process of chain polymerization. It is also important that we can fabricate conjugated polymer nanowires on semiconducting substrates that can be used as templates for exploring physics in 1-D systems. These results are a crucial step toward realization of molecular devices on various substrates.

METHODS

In this report, we use HOPG (ZYH grade, SPI Supplies) and MoS_2 (SPI Supplies) as the substrates. The deposition of an ordered molecular layer is carried out by drop-casting a 2 μL solution of 0.15 g/L 10,12-nonacosadiynoic acid (Tokyo Chemical Industry Co., Ltd.) in chloroform on a freshly cleaved substrate surface at room temperature. The substrate is then dried for 12−15 h in a desiccator at room temperature. All STM images are recorded using Nanoscope E system (Vecco Instruments Inc.) with constant tunneling current of 50 pA and sample

bias voltage of −1 V unless specified at ambient conditions (295 K). A wave generator (WF 1945, NF corporation) is employed to apply voltage pulses of required magnitude V_s and width (typically 5 μs) to the samples.

Supporting Information Available: Details of calculation for the reaction probability of chain polymerization. This material is available free of charge *via* the Internet at http://pubs.acs.org.

REFERENCES AND NOTES

1. Okawa, Y.; Aono, M. Nanoscale Control of Chain Polymerization. *Nature* **2001,** *409*, 683–684.
2. Okawa, Y.; Aono, M. Linear Chain Polymerization Initiated by a Scanning Tunneling Microscope Tip at Designated Positions. *J. Chem. Phys.* **2001,** *115*, 2317–2322.
3. Takajo, D.; Okawa, Y.; Hasegawa, T.; Aono, M. Chain Polymerization of Diacetylene Compound Multilayer Films on the Topmost Surface Initiated by a Scanning Tunneling Microscope Tip. *Langmuir* **2007,** *23*, 5247–5250.
4. Miura, A.; Feyter, S. D.; Abdel-Mottaleb, M. M. S.; Gesquière, A.; Grim, P. C. M.; Moessner, G.; Sieffert, M.; Klapper, M.; Müllen, K.; Schryver, F. C. D. Light- and STM-Tip-Induced Formation of One-Dimensional and Two-Dimensional Organic Nanostructures. *Langmuir* **2003,** *19* 6474–6482.
5. Takami, K.; Kuwahara, Y.; Ishii, T.; Akai-Kasaya, M.; Saito, A.; Aono, M. Significant Increase in Conductivity of Polydiacetylene Thin Film Induced by Iodine Doping. *Surf. Sci.* **2005,** *591*, L273–L279.
6. Akai-Kasaya, M.; Yamamoto, Y.; Saito, A.; Aono, M.; Kuwahara, Y. Polaron Injection into One-Dimensional Polydiacetylene Nanowire. *Jpn. J. Appl. Phys.* **2006,** *45* 2049–2052.
7. Scott, J. C.; Samuel, J. D. J.; Hou, J. H.; Rettner, C. T.; Miller, R. D. Monolayer Transistor Using a Highly Ordered Conjugated Polymer as the Channel. *Nano Lett.* **2006,** *6*, 2916–2919.
8. Akai-Kasaya, M.; Shimizu, K.; Watanabe, Y.; Saito, A.; Aono, M.; Kuwahara, Y. Electronic Structure of a Polydiacetylene Nanowire Fabricated on Highly Ordered Pyrolytic Graphite. *Phys. Rev. Lett.* **2003,** *25*, 255501-1–255501-4.
9. Giridharagopal, R.; Kelly, K. F. Substrate-Dependent Properties of Polydiacetylene Nanowires on Graphite and MoS_2. *ACS Nano* **2008,** *2*, 1571–1580.
10. Wang, Y.; Yang, K.; Wang, X.; Nagarajan, R.; Samuelson, L. A.; Kumar, J. *In Situ* Polymerization of Amphiphilic Diacetylene for Hole Transport in Solid State Dye-Sensitized Solar Cells. *Org. Electron* **2006,** *7*, 546–550.
11. Donhauser, Z. J.; Mantooth, B. A.; Kelly, K. F.; Bumm, L. A.; Monnell, J. D.; Stapleton, J. J.; Price, D. W., Jr.; Allara, D. L.; Tour, J. M.; Weiss, P. S. Conductance Switching in Single Molecules through Conformational Changes. *Science* **2001,** *292*, 2303–2307.
12. Moore, A. M.; Dameron, A. A.; Mantooth, B. A.; Smith, R. K.; Fuchs, D. J.; Ciszek, J. W.; Maya, F.; Yao, Y. X.; Tour, J. M.; Weiss, P. S. Molecular Engineering and Measurements To Test Hypothesized Mechanisms in Single Molecule Conductance Switching. *J. Am. Chem. Soc.* **2006,** *128* 1959–1967.
13. Solomon, G. C.; Herrmann, C.; Hansen, T.; Mujica, V.; Ratner, M. A. Exploring Local Currents in Molecular Junctions. *Nat. Chem.* **2010,** *2*, 223–228.
14. Joachim, C.; Gimzewski, J. K.; Aviram, A. Electronics Using Hybrid-Molecular and Mono-Molecular Devices. *Nature* **2000,** *408*, 541–548.
15. Park, J.; Pasupathy, A. N.; Goldsmith, J. I.; Chang, C.; Yaish, Y.; Petta, J. R.; Rinkoski, M.; Sethna, J. P.; Abruña, H. D.; McEuen, P. L.; *et al.* Coulomb Blockade and the Kondo Effect in Single-Atom Transistors. *Nature* **2002,** *417*, 722–725.
16. Liang, W.; Shores, M. P.; Bockrath, M.; Long, J. R.; Park, H. Kondo Resonance in a Single-Molecule Transistor. *Nature* **2002,** *417*, 725–729.
17. Piva, P. G.; DiLabio, G. A.; Pitters, J. L.; Zikovsky, J.; Rezeq, M.; Dogel, S.; Hofer, W. A.; Wolkow, R. A. Field Regulation of Single-Molecule Conductivity by a Charged Surface Atom. *Nature* **2005,** *435*, 658–661.
18. Díez-Pérez, I.; Hihath, J.; Lee, Y.; Yu, L.; Adamska, L.; Kozhushner, M. A.; Oleynik, I. I.; Tao, N. Rectification and Stability of a Single Molecular Diode with Controlled Orientation. *Nat. Chem.* **2009,** *1*, 635–641.
19. Song, H.; Kim, Y.; Jang, Y. H.; Jeong, H.; Reed, M. A.; Lee, T. Observation of Molecular Orbital Gating. *Nature* **2009,** *462*, 1039–1043.
20. Scott, G. D.; Natelson, D. Kondo Resonances in Molecular Devices. *ACS Nano* **2010,** *4*, 3560–3579.
21. Aviram, A.; Ratner, M. A. Molecular Rectifiers. *Chem. Phys. Lett.* **1974,** *29*, 277–283.
22. Enkelmann, V. Structural Aspects of the Topochemical Polymerization of Diacetylenes. *Adv. Polym. Sci.* **1984,** *63*, 91–136.
23. Rahe, P.; Nimmrich, M.; Greuling, A.; Schtte, J.; Star, I. G.; Rybacek, J.; Angeles, G. H.; Star, I.; Rohlfing, M.; Khünle, A. Toward Molecular Nanowires Self-Assembled on an Insulating Substrate: Heptahelicene-2-carboxylic acid on Calcite ($10\bar{1}4$). *J. Phys. Chem. C* **2010,** *114*, 1547–1552.
24. McMenamin, J. C.; Spicer, W. E. Photoemission Studies of Layered Transition-Metal Chalcogenides: MoS_2. *Phys. Rev. B* **1977,** *16*, 5474–5487.
25. Giancarlo, L. C.; Fang, H.; Rubin, S. M.; Bront, A. A.; Flynn, G. W. Influence of the Substrate on Order and Image Contrast for Physisorbed, Self-Assembled Molecular Monolayers: STM Studies of Functionalized Hydrocarbons on Graphite and MoS_2. *J. Phys. Chem. B* **1998,** *102* 10255–10263.
26. Groszek, A. J. Preferential Adsorption of Long-Chain Normal Paraffins on MoS_2, WS_2, and Graphite from *n*-Heptane. *Nature* **1964,** *204*, 680.
27. Cincotti, S.; Rabe, J. P. Self-Assembled Alkane Monolayers on $MoSe_2$ and MoS_2. *Appl. Phys. Lett.* **1993,** *62* 3531–3533.
28. Okawa, Y.; Takajo, D.; Tsukamoto, S.; Hasegawa, T.; Aono, M. Atomic Force Microscopy and Theoretical Investigation of the Lifted-up Conformation of Polydiacetylene on a Graphite Substrate. *Soft Matter* **2008,** *4*, 1041–1047.
29. Lastapis, M.; Martin, M.; Riedel, D.; Hellner, L.; Comtet, G.; Dujardin, G. Picometer-Scale Electronic Control of Molecular Dynamics Inside a Single Molecule. *Science* **2005,** *308*, 1000–1003.
30. Bellec, A.; Riedel, D.; Dujardin, G; Boudrioua, O.; Chaput, L.; Stauffer, L.; Sonnet, Ph. Nonlocal Activation of a Bistable Atom through a Surface State Charge-Transfer Process on Si(100)-(2 × 1):H. *Phys. Rev. Lett.* **2010,** 048302-1–048302-4.
31. Hipps, K. W.; Mazur, U. Unoccupied Orbital Mediated Tunneling: Resonance-like Structures in the Tunneling Spectra of Polyacenes. *J. Phys. Chem.* **1994,** *98* 5824–5829.
32. Mazur, U.; Hipps, K. W. Orbital-Mediated Tunneling, Inelastic Electron Tunneling, and Electrochemical Potentials for Metal Phthalocyanine Thin Films. *J. Phys. Chem. B* **1999,** *103*, 9721–9727.
33. Hipps, K. W.; Barlow, D. E.; Mazur, U. Orbital Mediated Tunneling in Vanadyl Phthalocyanine Observed in both Tunnel Diode and STM Environments. *J. Phys. Chem. B* **2000,** *104*, 2444–2447.
34. Barlow, D. E.; Scudiero, L.; Hipps, K. W. Scanning Tunneling Microscopy Study of the Structure and Orbital-Mediated Tunneling Spectra of Cobalt(II) Phthalocyanine and Cobalt(II) Tetraphenylporphyrin on Au(111): Mixed Composition Films. *Langmuir* **2004,** *20*, 4413–4421.
35. Chance, R. R.; Patel, G. N. Solid-State Polymerization of a Diacetylene Crystal: Thermal, Ultraviolet, and γ-ray Polymerization of 2,4-Hexadiyne-1,6-Diol Bis-(*p*-toluene sulfonate). *J. Polym. Sci., Polym. Phys. Ed.* **1978,** *16*, 859–881.
36. Bertault, M.; Fave, J. L.; Scott, M. The Lowest Triplet State of a Diacetylene. *Chem. Phys. Lett.* **1979,** *62*, 161–165.
37. Neumann, W.; Sixl, H. The Mechanism of the Low Temperature Polymerization Reaction in Diacetylene Crystals. *Chem. Phys.* **1981,** *58*, 303–312.

38. Léger, A.; Klein, J.; Belin, M.; Defourneau, D. Electronic Transitions Observed by Inelastic Electron Tunneling Spectroscopy. *Solid State Commun.* **1972,** *11*, 1331–1335.
39. Hipps, K. W.; Mazur, U. Inelastic Electron Tunneling: An Alternative Molecular Spectroscopy. *J. Phys. Chem.* **1993,** *97*, 7803–7814.